



NRC Publications Archive Archives des publications du CNRC

Rheology and extrusion foaming of chain-branched poly(lactic acid) Mihai, Mihaela; Huneault, Michel A.; Favis, Basil D.

This publication could be one of several versions: author's original, accepted manuscript or the publisher's version. /
La version de cette publication peut être l'une des suivantes : la version prépublication de l'auteur, la version
acceptée du manuscrit ou la version de l'éditeur.

For the publisher's version, please access the DOI link below. / Pour consulter la version de l'éditeur, utilisez le lien
DOI ci-dessous.

Publisher's version / Version de l'éditeur:

<https://doi.org/10.1002/pen.21561>

Polymer Engineering and Science, 50, 3, pp. 629-642, 2010-03-15

NRC Publications Record / Notice d'Archives des publications de CNRC:

<https://nrc-publications.canada.ca/eng/view/object/?id=9d3f233b-a476-4342-aae9-3d736f0d02c1>

<https://publications-cnrc.canada.ca/fra/voir/objet/?id=9d3f233b-a476-4342-aae9-3d736f0d02c1>

Access and use of this website and the material on it are subject to the Terms and Conditions set forth at

<https://nrc-publications.canada.ca/eng/copyright>

READ THESE TERMS AND CONDITIONS CAREFULLY BEFORE USING THIS WEBSITE.

L'accès à ce site Web et l'utilisation de son contenu sont assujettis aux conditions présentées dans le site

<https://publications-cnrc.canada.ca/fra/droits>

LISEZ CES CONDITIONS ATTENTIVEMENT AVANT D'UTILISER CE SITE WEB.

Questions? Contact the NRC Publications Archive team at

PublicationsArchive-ArchivesPublications@nrc-cnrc.gc.ca. If you wish to email the authors directly, please see the
first page of the publication for their contact information.

Vous avez des questions? Nous pouvons vous aider. Pour communiquer directement avec un auteur, consultez la
première page de la revue dans laquelle son article a été publié afin de trouver ses coordonnées. Si vous n'arrivez
pas à les repérer, communiquez avec nous à PublicationsArchive-ArchivesPublications@nrc-cnrc.gc.ca.



Rheology and Extrusion Foaming of Chain-Branched Poly(lactic acid)

Mihaela Mihai,^{1,2} Michel A. Huneault,¹ Basil D. Favis²

¹ Industrial Materials Institute, National Research Council of Canada, Boucherville, Québec, Canada J4B 6Y4

² CREPEC, Chemical Engineering Department, École Polytechnique de Montréal, Montréal, Québec, Canada H3C 3A7

In this study, the effect of macromolecular chain-branching on poly(lactic acid) (PLA) rheology, crystallization, and extrusion foaming was investigated. Two PLA grades, an amorphous and a semi-crystalline one, were branched using a multifunctional styrene-acrylic-epoxy copolymer. The branching of PLA and its foaming were achieved in one-step extrusion process. Carbon dioxide (CO₂), in concentration up to 9%, was used as expansion agent to obtain foams from the two PLA branched using chain-extender contents up to 2%. The foams were investigated with respect to their shear and elongational behavior, crystallinity, morphology, and density. The addition of the chain-extender led to an increase in complex viscosity, elasticity, elongational viscosity, and in the manifestation of the strain-hardening phenomena. Low-density foams were obtained at 5–9% CO₂ for semi-crystalline PLA and only at 9% CO₂ in the case of the amorphous PLA. Differences in foaming behavior were attributed to crystallites formation during the foaming process. The rheological and structural changes associated with PLA chain-extension lowered the achieved crystallinity but slightly improved the foamability at low CO₂ content. POLYM. ENG. SCI., 50:629–642, 2010. © 2009 Society of Plastics Engineers

INTRODUCTION

Poly(lactic acid) (PLA) is an aliphatic polyester first used in medical applications and now in the industrial packaging field. It is a rigid, brittle, and transparent bio-based polymer and can be obtained from ring-opening polymerization of lactide, a lactic acid dimer. PLA is often compared with poly(ethylene terephthalate) (PET) in terms of its tensile strength, elastic modulus, impact resistance, and barrier properties [1, 2]. It can be transformed using extrusion and molding technologies [3]. PLA crys-

tallinity can be controlled by adjusting the content of its two stereoisomers, L-LA and D-LA. The PLLA crystallinity can attain around 45%. This crystallinity level decreases with D-LA content and molecular weight [4].

The extrusion foaming process includes a sequence of complex phenomena. First, the blowing agent must be dissolved under pressure into the polymer leading to the plasticization of the polymer melt. When the polymer-blowing agent solution emerges from the die, the pressure drop causes phase separation and nucleation of gas cells. These cells undergo a growth stage fueled by the diffusion of the blowing agent from the polymer matrix into these newly formed gas cells. The next step is the foam stabilization which depends on nonlinear viscoelastic property (strain-hardening), polymer deplasticization (i.e., the separation by diffusion of blowing agent phase out from polymer phase), polymer crystallization, and cooling rate [5, 6]. The strain-hardening is a rapid extensional viscosity increase in time that occurs when the polymer melt is highly oriented, i.e., during the cell growth stage in the particular case of polymer foaming. The strain-hardening is observed when the macromolecular chain disentanglement rate is too low in relation with the deformation rate. In linear polymers, the incorporation of long chain branches or the addition of a low fraction of high molecular weight polymer has been used to create strain-hardening and to enhance the foaming process [7–11]. At first glance, PLA rheology is not well suited for the foaming process because it has a relatively low melt strength and typically does not exhibit any strain-hardening. A further drawback of PLA is that it has a poor thermal stability and can undergo chain-scission during processing [12, 13]. Therefore, in comparison with polymers such as polyethylene, polypropylene or polystyrene, the PLA requires substantially larger molecular weight to display similar melt viscoelastic behavior at a given temperature [14]. When the chain architecture of PLA is changed from linear to star or branched, then zero-shear viscosity and elasticity increase, the shear-thinning behavior is accentuated and relaxation time is increased which should be favorable to foam stabilization [15–18].

Correspondence to: Michel A. Huneault; e-mail: michel.huneault@cnrc-nrc.gc.ca

DOI 10.1002/pen.21561

Published online in Wiley InterScience (www.interscience.wiley.com).

© 2009 Society of Plastics Engineers



FIG. 1. Screw configuration used in extrusion foaming of PLA.

There are very few studies about extrusion foaming of PLA [19–21]. Amorphous and semi-crystalline PLA were foamed by extrusion using the CO_2 as blowing agent. Low-density foams, with densities in the 20–30 kg/m^3 range, were achieved when the CO_2 concentration exceeded a threshold of around 7%. The foam crystallinity was shown to vary depending on D-LA content, CO_2 concentration, polymer flow rate, and die diameter.

The literature is also very scarce with respect to elongational viscosity of PLA. During elongation of PLA, strain-hardening was reported and was associated to the presence of a low fraction of high molecular PLA in the sample [22]. It was also showed that the addition of small amounts of PDLA could lead to strain-hardening in PLLA melts [23]. In this case, the stereocomplex formation acted as crosslink points and resulted in physical branching of the PLA chains. This effect was stronger when PDLA of low molecular weight was used.

Chemical chain-extension is largely used to increase the melt strength and elasticity of linear polymers. For polyesters, chain-extension consists in increasing the molecular weight by bridging the hydroxyl or carboxyl reactive-end groups using bi or poly-functional molecules. For PET, branching was obtained by reaction with pyromellitic dianhydride, [24–26], and with various epoxy-based chain-extenders, [27–31]. For PLA, various diisocyanate were investigated for this purpose [32–39]. All these bifunctional molecules have a narrow processing window and can lead to gel formation. Long-random copolymers with multiple reactive sites are another approaches for producing chain-branched structures. For example, ethylene-methyl acrylate-glycidyl methacrylate copolymers have successfully been used for the branching of PET [40]. Recently, a multifunctional styrene-acrylic-epoxy random oligomer, with a molecular weight around 3000 g/mol, has been proposed as chain-extender without the aforementioned limitations [41, 42].

In this study, we investigated extrusion foaming and rheology of chain-branched PLA. The branching was done using the abovementioned multifunctional styrene-acrylic-epoxy copolymer. Extrusion foaming of two PLA grades, one amorphous, and one semi-crystalline was carried out using the CO_2 as blowing agent. The objective of this work was to establish a relationship between the foaming behavior, crystallization, and the rheological behavior of chain-branched PLA. The effect of the chain-extender and blowing agent content on crystallinity and foam morphology and microstructure are discussed.

EXPERIMENTAL

Materials

Two different PLA grades supplied by NatureWorks were used in this study. PLA8302D was an amorphous grade (aPLA) and PLA4032D was a semi-crystalline grade (cPLA), with approximately 10 and 2%, respectively of D-lactic acid monomer. The chain-extender (CE), CesaExtend OMAN698493 from Clariant Additive Masterbatches, was an epoxy-styrene-acrylic oligomer, provided in masterbatch form in a PLA carrier. The epoxy groups are believed to react preferentially with the carboxyl-end groups of the PLA chains to form a branched structure. The hydroxyl-terminal groups of PLA are less reactive with the epoxy groups and should remain substantially unreacted. This should avoid crosslinking and gel formation [41, 42]. The PLA and CE were dried at 55°C for a minimum of 8 h prior to use. CO_2 with a purity of 99.9% was used as blowing agent in the PLA foam extrusion process.

Internal Mixer

Mixing of CE with the PLA was generally carried in the twin-screw extrusion foaming experiments but, in one selected experiment, an internal mixer with a mixing volume of 60 cm^3 was used to make blends from cPLA with different CE contents between 0.2 and 2%. The blends were obtained under N_2 atmosphere for a blending time of 20 min at 200°C and a screw rotation speed of 80 rpm. After blending, the samples were quenched in cold water to avoid crystallization during cooling.

Extrusion Foaming Process

A Leistritz 34 mm co-rotating twin-screw extruder comprising 12 barrel zones was used to prepare the PLA foams. The process configuration is presented in Fig. 1. The screw configuration in the first part of the extruder was dedicated to the chain-branching reaction where the temperature was maintained at around 190°C for all the formulations. The CO_2 was pumped into barrel segment 7 using a high-precision injection pump. This second part of the extruder was used to solubilize the blowing agent in the polymer melt and to bring the material temperature down to the desired final extrusion foaming temperature.

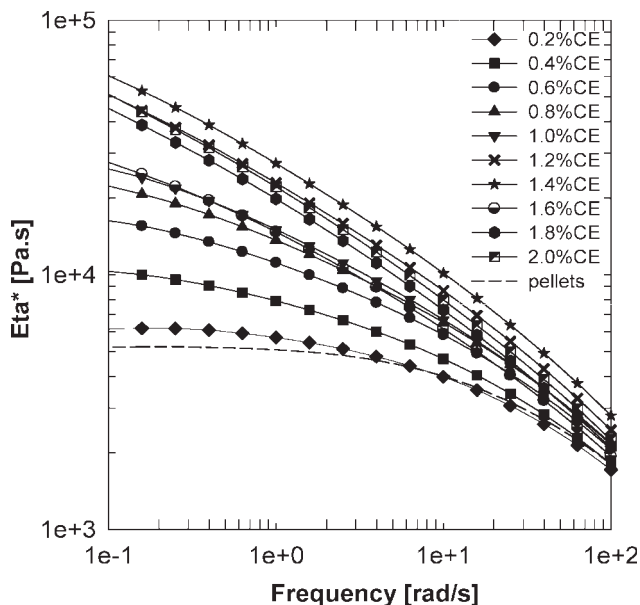


FIG. 2. Viscosity of cPLA at 180°C branched with different contents of CE. The branching was carried out in an internal mixer at 200°C for a mixing time of 20 min.

The temperature profile in this second part of the extruder was decreased as a function of the formulation with the purpose to obtain the optimal foam and this profile will be presented and discussed in detail in the article. A pair of reverse screw elements, situated upstream from the blowing agent injection point, was used as a dynamic melt seal to maintain a high CO₂ pressure in the latter portion of the extruder. A gear pump was also placed at the end of the extrusion line to preserve a high-pressure level at the end of the extruder. The extruder was operated at a constant screw rotation speed of 150 rpm and at a constant flow rate of 10 kg/h. A capillary die with a 2 mm diameter was used. All foam samples were stored for 2 weeks at room temperature prior to crystallinity measurement to make sure the CO₂ had diffused out of the samples. The samples were dimensionally stable during that period.

Rheological Measurements

Sample Preparation. Rheological measurements were carried out on extruded materials (unfoamed or foamed) unless stated otherwise. The foamed material was cut in small pieces, dried for 12 h at 55°C, and re-extruded at 180°C using a mini-extruder (Haake Thermal Mixing) under N₂ atmosphere. This extrusion step was necessarily to break down the foam structure and to obtain homogeneous samples for rheological measurements. In the case of unfoamed samples, this extrusion step was applied with the purpose to have the same thermal treatment as for the foamed samples. After the extrusion step, all samples were dried again for 12 h at 55°C prior to rheological testing. Similar viscosities were found for controls extruded with the twin-screw extruder and the mini-

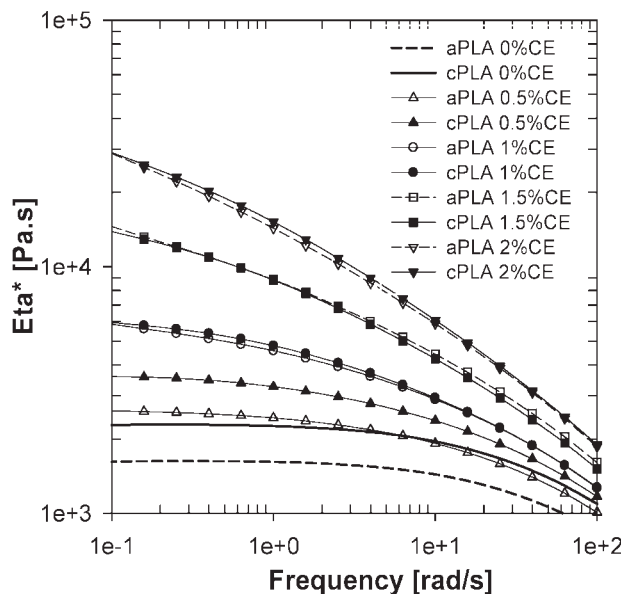


FIG. 3. Viscosity of branched aPLA and cPLA at 180°C branched with 0, 0.5, 1, 1.5, and 2% CE. The branching was carried out in the twin-screw extruder at 180°C.

extruder indicating that the extra thermal history in the mini-extruder did not degrade the material.

Dynamic Mode. The complex viscosity was measured in plate–plate geometry at 180°C in a dynamic mode using an Ares rotational rheometer from TA Instrument's. The complex viscosity was first monitored over time to verify the thermal stability of the samples. Frequency sweeps were carried out to determine the complex viscosity over a frequency ranging from 0.1 to 100 rad/s. The tests were conducted for a deformation of 15%. The sam-

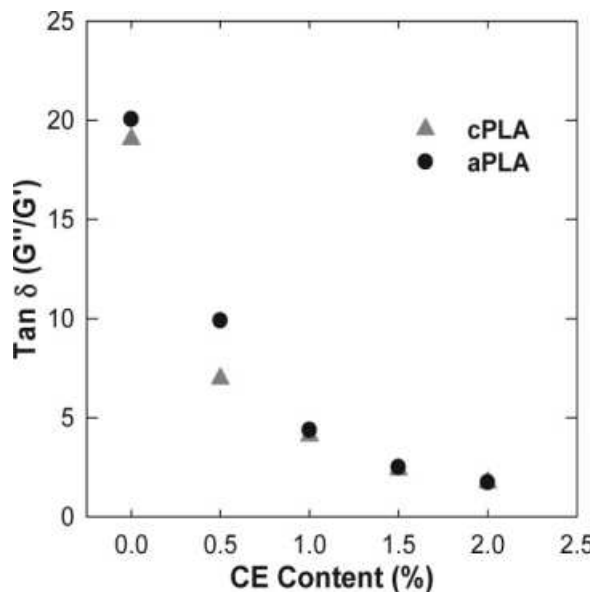


FIG. 4. Tan δ as a function of CE concentration for a frequency of 1 rad/s for branched-extruded aPLA and cPLA.

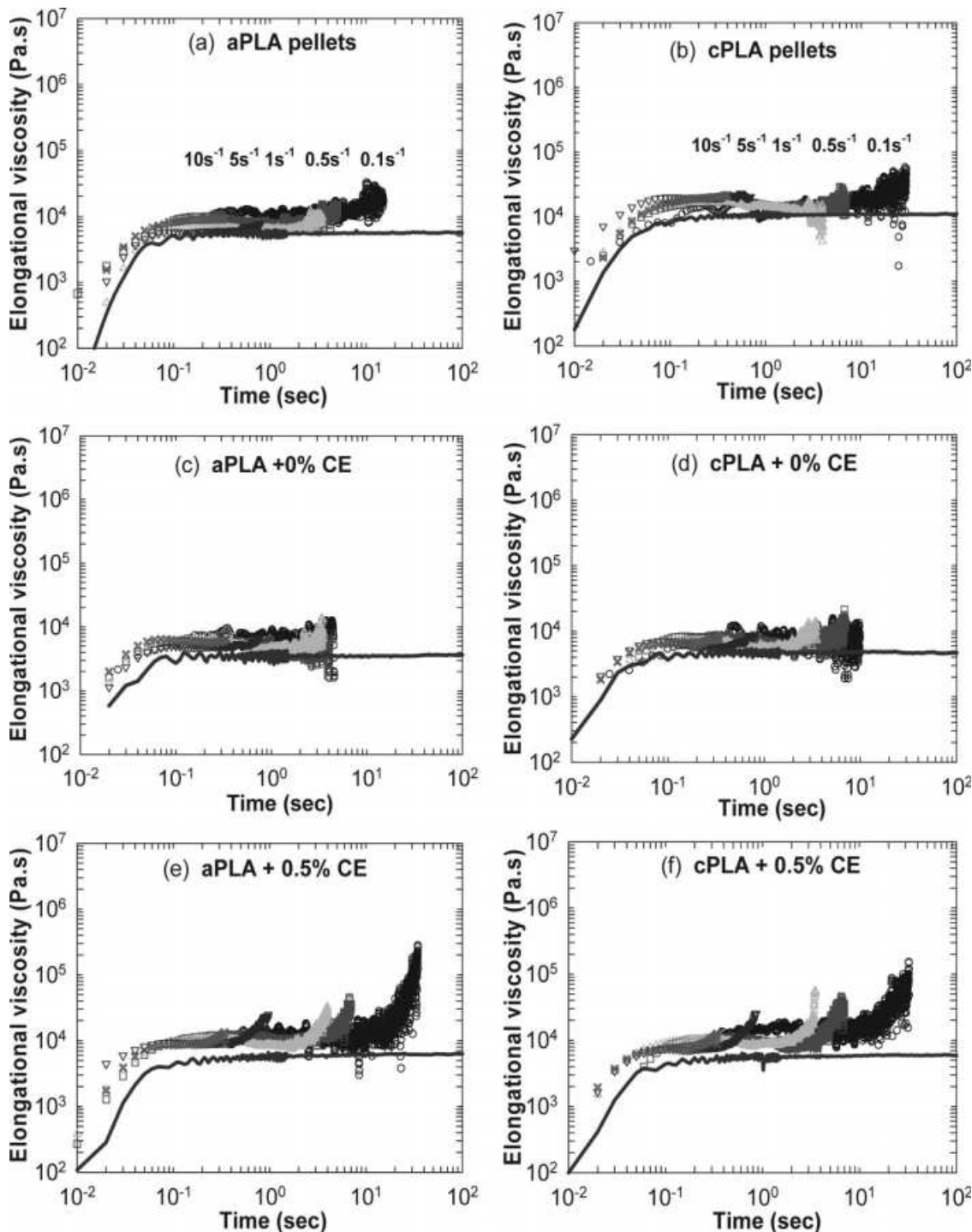


FIG. 5. Elongational viscosity as a function of time of virgin aPLA and cPLA (a and b), extruded (c and d), and branched with up to 2% chain extender (e–l). Strain rates were 0.1, 0.5, 1, 5, and 10 s^{-1} from right to the left. The continuous curves represent the stress growth functions ($3\eta^+$) obtained in shear.

ples were kept under a nitrogen blanket during testing to minimize oxidation and to maintain a dry environment.

Elongation Mode

The elongational viscosity was measured at 180°C using SER-HV-A01 Universal Testing Platform for the

TA Instrument's Ares rotational rheometer [43, 44]. The samples were compression molded to dimensions of $18 \times 10 \times 1 \text{ mm}^3$ and were dried again at 55°C for 12 h before elongational testing. For each sample, the torque was monitored as a function of time for five different Hencky strain rates: 0.1, 0.5, 1, 5, and 10 s^{-1} . The maximum Hencky strain was constant at 3.5 and, therefore,

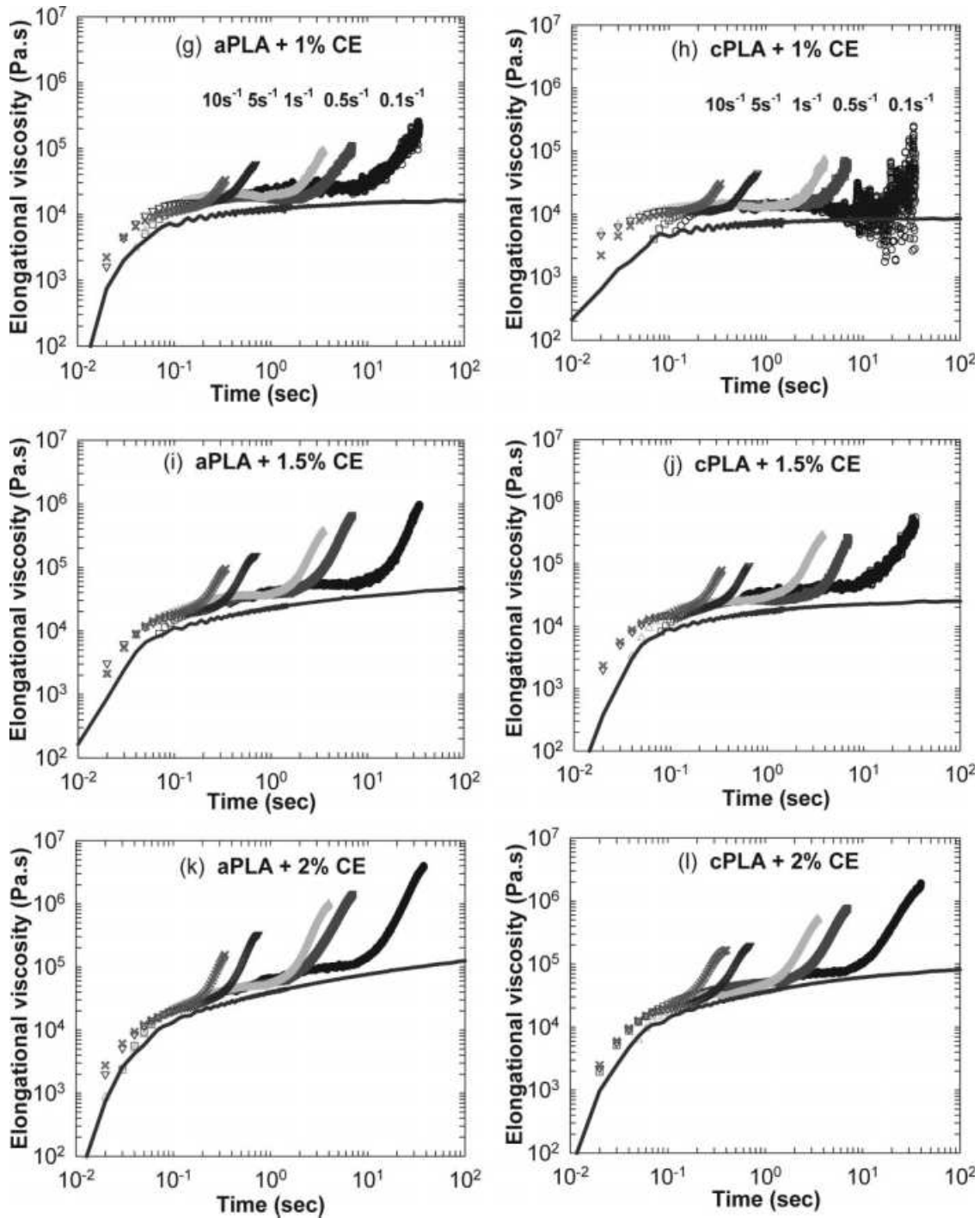


FIG. 5. (Continued)

the duration of each test was 35, 7, 3.5, 0.7, and 0.35 s, respectively. The following equation was used to calculate the tensile stress growth function for molten PLA in steady extension [43, 44]:

$$\eta_E^+ = \frac{(T)}{2R\dot{\epsilon}_H A_0 (\rho_S / \rho_M)^{2/3} \exp(-\dot{\epsilon}_H [t])} \quad (1)$$

where η_E^+ is the value of tensile stress growth, $\dot{\epsilon}_H$ is the applied Hencky strain rate, T is the torque, R is the drum

radius, A_0 is initial area of the sample measured in the solid state, and t is time data. The density of PLA in solid state, ρ_S , was considered 1.25 g/cm^3 [1], and the value for PLA melt at 180°C , ρ_M , was 1.115 g/cm^3 [45].

Crystallization

Differential Scanning Calorimetry (DSC) analysis was carried out on dry unfoamed and foamed samples using a TA Instrument's Q1000 apparatus calibrated using an in-

dium standard. For the initial crystallization measurements, the samples were heated from 30 to 200°C at 20°C/min and the enthalpy of crystallization upon heating ΔH_c and melting enthalpy ΔH_m were measured. The initial crystalline content in the samples was given by $(\Delta H_m - \Delta H_c)/\Delta H_f$ where ΔH_f is the theoretical heat of fusion of 100% crystalline PLA. A value of 93 J/g was taken for PLAs theoretical heat of fusion [46]. After the initial crystallinity measurements, the samples were maintained at 200°C for 2 min to erase the thermal history, cooled to 30°C at 20°C/min and then reheated to 200°C at 20°C/min.

Foam Characterization

The cryogenically fractured foam surfaces, perpendicular to the extrusion direction, were observed on a Scanning Electron Microscope (SEM). All foamed surfaces were sputter-coated with platinum prior to the observation. The density of the foam was determined by a water displacement method. Cell population density (n) was calculated as the number of cells per unit volume with respect to the unfoamed PLA. The number of cells (n_b) in a defined area ($l \times l$) was first calculated from SEM micrographs and then the total number of cells per cubic centimeter was calculated with the equation:

$$n = (n_b/l^2)^{3/2} \cdot v_a \text{ where } v_a = \rho_{\text{PLA}}/\rho_{\text{foam}} \quad (2)$$

where v_a is the radial expansion ratio, ρ_{PLA} and ρ_{foam} are the density of unfoamed and foamed PLA respectively.

RESULTS AND DISCUSSION

The effect of CE addition on PLA viscosity was first evaluated on blends prepared in the internal mixer. Figure 2 presents the complex viscosity as a function of frequency for cPLA blended with different CE contents. The cPLA pellets used as reference showed the lowest zero-shear viscosity, around 5×10^3 Pa s, and a well-defined Newtonian plateau for frequencies below 10 rad/s. The viscosity increased with CE content for concentrations up to 1.4%. For an oscillation rate of 0.1 rad/s, the viscosity increased by one order of magnitude and the Newtonian plateau disappeared in the investigated frequency range. This change in viscosity was a clear indication of the macromolecular chain-extension and confirmed the efficiency of the investigated chain-extender. For CE contents from 1.4 to 2% CE, the viscosity decreased but remained close to the maximum value obtained for 1.4% CE curve. This implies that a threshold of CE concentration was reached and that no more carboxyl-end groups were available on cPLA chains to further react with the epoxy moieties of the excess chain-extender.

The internal mixing was carried out for 20 min, leaving ample time for the completion of the branching reaction. These experiments were reproduced using the twin-screw extrusion process to verify if a similar viscosity increase could be obtained regardless with the much shorter residence time encountered in a continuous extrusion process. Figure 3 presents the complex viscosity as a function of frequency for extruded PLA samples. The extruded unbranched aPLA and cPLA, presented as a reference, showed a well-defined Newtonian plateau with the lowest zero-shear viscosities at 1600 and 2300 Pa s, respectively. Comparing with the virgin material (see Fig. 2), the viscosity of the extruded cPLA was decreased by a half due to the thermal and mechanical degradation that occurred during extrusion. At 0.5% CE, the zero-shear viscosity increased to 2600 and 3600 Pa s, respectively. Increasing CE content up to 2% led to a continuous rise of viscosity and to an accentuation of the shear-thinning behavior. At these CE concentrations, the two PLA grades showed almost identical viscosity curves. The viscosity values observed for extruded samples were slightly smaller in comparison to those obtained by internal mixing (see Fig. 2) but still showed a significant viscosity increase in relation to the reference materials. The lower viscosity for extruded samples could be explained by the shorter reaction time in extrusion, about 2–3 min versus 20 min in internal mixer, and by a greater chain-scission due to the more aggressive mixing environment found in the extrusion process. It is noteworthy that the higher chain-scission encountered in the extrusion process probably led at the formation of a higher number of carboxyl groups than in internal mixing. In turn, this has pushed the CE concentration threshold observed in Fig. 2 to a higher level.

Figure 4 presents $\tan \delta$ of aPLA and cPLA measured at 180°C as a function of CE content for a frequency of 1 rad/s. $\tan \delta$ is defined as the ratio of G''/G' and is therefore a ratio of viscous to elastic contribution at a given oscillation frequency. $\tan \delta$ of the extruded PLA (0% CE) was around 20. This value decreased continuously down to a value around 4 at increasing CE concentration from 0 to 2%. A decrease in $\tan \delta$ is indicative of the increase in melt elasticity. It can be assumed that increased number of branches with CE content has increased the number of entanglements between PLA macromolecular chains and is an additional evidence of the branching efficiency of the investigated chain-extender.

The chain-extension of PLA should also reflect into the material response to an elongation deformation. Figure 5 compares the transient elongational viscosity of aPLA and cPLA at 180°C with up to 2% CE. The elongational viscosity of PLA pellets, (a) and (b), and the viscosity of the extruded materials without chain-extender, (c) and (d), were presented as references. As in shear experiments, the extruded unbranched PLA showed a lower elongational viscosity than the pellets due to the chain-scission that

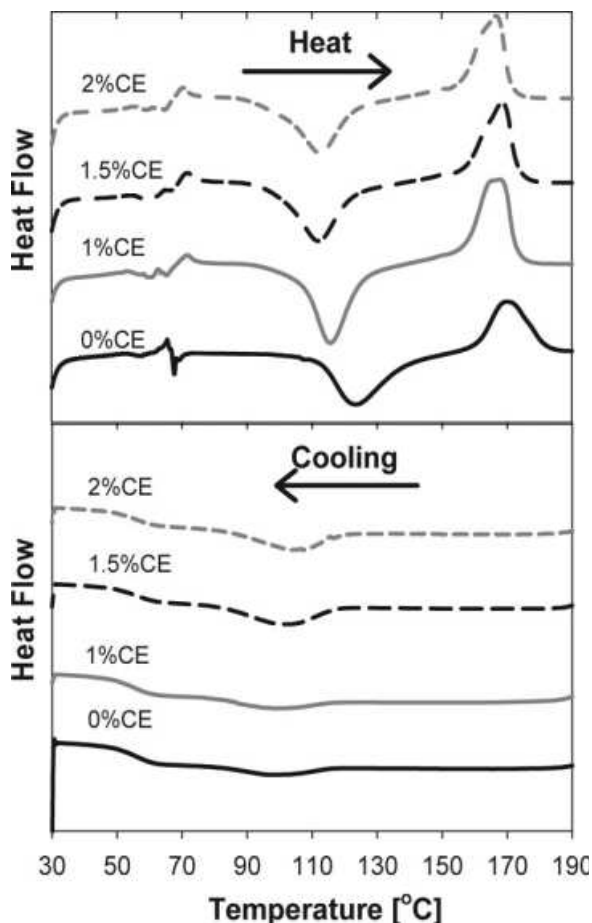


FIG. 6. DSC scans obtained during the first heating (+20°C/min) and the cooling (-20°C/min) for branched and unfoamed cPLA samples.

occurred during the extrusion. The reference materials did not exhibit any strain-hardening. The samples also broke prematurely before the maximum extension enabled by the test (i.e., Hencky strain of 3.5). The cPLA resisted up to a longer extension than aPLA. By contrast, all samples with 0.5–2% CE, (e) to (l), resisted to the elongational deformation without failure for the complete test durations and displayed strain-hardening. Some instability upon elongational deformation was found at the low strain rate of 0.1 s^{-1} due to the low force levels involved. In general, the elongational viscosity and the magnitude of the strain-hardening increased with CE content. The aPLA and cPLA showed very similar behaviors. At 1.5 and 2% CE, the strain-hardening led to an increase in viscosity by two orders of magnitude. The shear stress growth function ($3\eta^+$) for each formulation, obtained at a low shear ($\dot{\gamma} = 0.005 \text{ s}^{-1}$), are also presented in Fig. 5. In general, the shear growth curves were close to the η_c^+ curves. The best superposition was obtained for the unmodified PLA. With the addition of the chain-extender, the shear growth curves were systematically lower than the η_c^+ curves. In other words, the Trouton law ($\eta_c^+ = 3\eta^+$) was not perfectly obeyed for the branched materials. A first explanation is that the Trouton law is valid for inelastic Newtonian fluids, while in the current situation important elastic component was present in the branched materials. Second, the Trouton law is valid only at a very low deformation rate, $\dot{\epsilon} = \dot{\gamma} = \omega \rightarrow 0$. Our stress growth functions in steady-shear were obtained at a deformation rate of 0.005 s^{-1} . It is possible that we were not yet in the Newtonian plateau region and that we slightly underestimated the shear stress growth curve. However, it was not possible to use a lower deformation rate because the measured stresses were below the accuracy limit of the apparatus.

It is important to verify how the chain-branching could affect the thermal behavior of PLA. Figure 6 presents DSC scans obtained during the first heating and during the cooling of unfoamed cPLA samples extruded with different levels of chain-extender. The energy associated to the crystallization exotherm was in all cases equal to the melting endotherm. Thus, the extruded samples did not show any initial crystallinity. This was expected because the extrudates were rapidly cooled immediately after die exit. The peak crystallization temperature on heating, T_{ch} , decreased by around 10°C as the CE content was increased up to 2%. All samples showed a similar melting peak, around 166°C. The crystallinity level developed on heating was around 40% for the unbranched cPLA and decreased to 30% at 2% CE. On cooling, the cPLA with 0–1% CE contents developed very low crystallinity levels, around 5%. The weak crystallization peaks on cooling, T_{cc} , appeared centered around 96°C. This peak increased in magnitude and was shifted up to 105°C as the CE content was increased up to 2%. The maximum crystallinity level achieved on cooling for the highly branched cPLA reached a maximum of 10%. From the obtained results, it seems that the rate of crystallization was increased in presence of the chain-extender. This is showed by the T_{ch} and T_{cc} shifts achieved on heating and cooling at increasing CE levels. It should be noted, however, that in this CE concentration range, the level of crystallinity achieved on heating was lower (30%) than in the extruded unmodified resin (40%). Therefore, the branching seemed to accelerate nucleation but, at the same time, disrupted the chain linearity and created steric hindrance that reduced the amount of PLA chains that could crystallize.

We will now examine the foamability of aPLA and cPLA and its relation with CE content. Figures 7 presents SEM micrographs of fractured surfaces of foam obtained with 5, 7, and 9% CO_2 while Table 1 shows the corresponding densities. The use of 3% CO_2 was not enough to foam the PLA and, hence, this formulation was discarded from the morphological characterization. The use of 5% CO_2 only led to high-density foams, in the 800–900 kg/m^3 range, as can be seen in Fig. 7a, d, and g. This is only slightly lower than unfoamed PLA (1250 kg/m^3). The foam cell walls were thick and foam cells did not contact one another. Surprisingly, the same foam morphology and density was obtained regardless of the CE content. At 7% CO_2 , Fig. 7b, e, and h, the foam density was decreased down to 200 kg/m^3 , the cell walls were

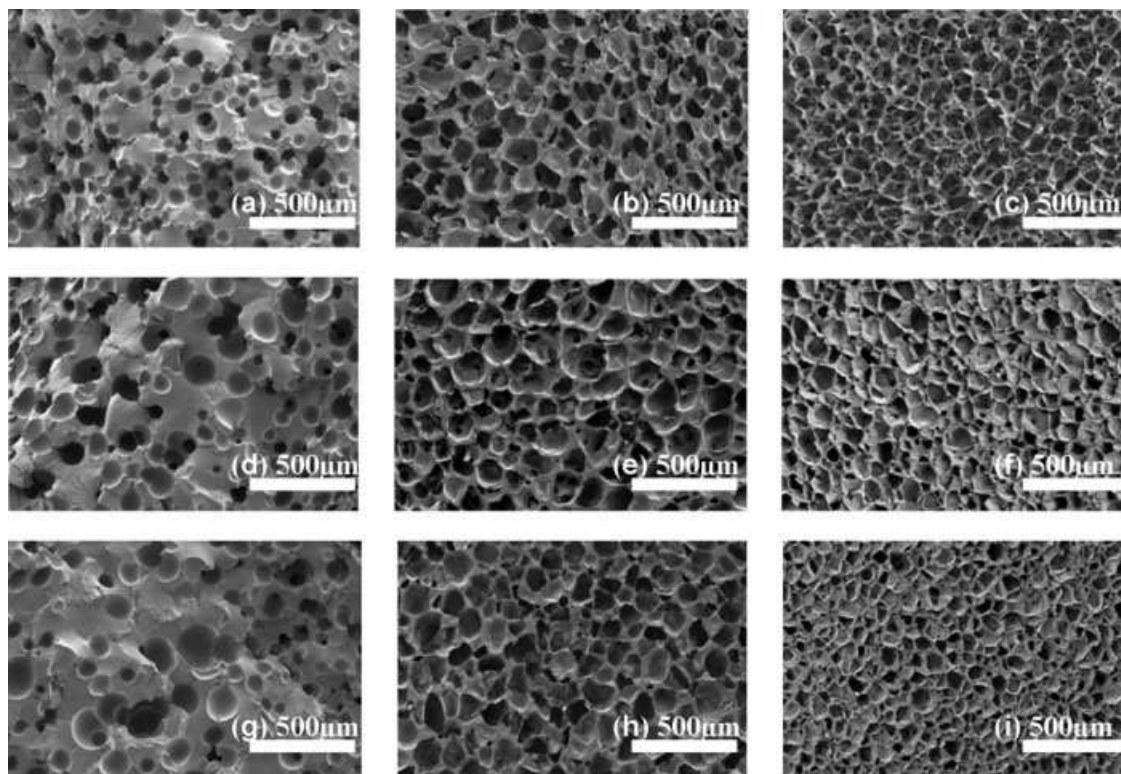


FIG. 7. SEM morphology of amorphous aPLA foams obtained with 5, 7, and 9% CO₂ (from left to right) and branched with 0, 1, and 2% CE (from top to bottom).

thinner, and the cell size distribution became more uniform, around 130 μm. Again, the CE content did not affect the foam quality. High-quality low-density foams were obtained only at 9% CO₂ for all levels of branching. The cells dimensions decreased to around 100 μm, as seen in micrographs (c), (f), and (i). The foam density decreased at 20 kg/m³. Hence, speaking in terms of foam morphology and density, the aPLA foams were not improved by the presence of the chain-extender content.

Figure 8 and Table 2 present respectively the morphologies and corresponding densities of cPLA foams obtained in the same conditions as for the aPLA foams. In contrast with aPLA, the cPLA foams exhibited lower densities and smaller cell sizes, especially at 5 and at 7% CO₂. At 5% CO₂, the density of unbranched cPLA was already as low as 65 kg/m³. As seen from Fig. 8, the foams obtained at 5% CO₂ showed an increase in cell dimension from 130 up to 300 μm and a decreased in foam density from 65 down to 36 kg/m³, with the increasing CE content. At 7 and 9% CO₂, similar morphologies were obtained for all CE contents. These foams showed higher cell densities, higher uniformities of cell dimensions of 100 μm, and foam densities around 30 kg/m³. Hence, the cPLA foam morphology and density were affected by the increase of the chain-extender content only at 5% CO₂. It could be assumed that the chain-branching resulted in better cell wall stabilization during growth only at low blowing agent concentration. In our

previous work, it was shown that cPLA can fully crystallize in a very short time during the foaming process in the presence of CO₂ when a critical threshold of 7% was exceeded [20, 21]. At higher blowing agent concentrations, it is possibly that foam crystallization plays a more important role in the foam nucleation and stabilization than the chain-branching. Therefore, it is interesting to investigate the effect of the chain-extender on the crystallization and foaming of branched cPLA foams.

Figure 9 presents DSC scans on heating of cPLA foams with 0% CE and 2% CE. At the time of testing, the CO₂ had completely diffused out of the samples. Thus, the DSC measurements were not affected by any CO₂ plasticization effect. All the samples presented some crystallization upon heating since the foams were only partially crystallized during the foaming process. For unmodified cPLA foamed samples, the peak crystallization temperature, T_{ch} , decreased from 118 to 92°C with increasing CO₂ concentration. At the same time, the level

TABLE 1. Density of aPLA foams.

CE content	Density (kg/m ³)		
	5% CO ₂	7% CO ₂	9% CO ₂
0%	940	210	27
1%	820	220	19
2%	900	190	19

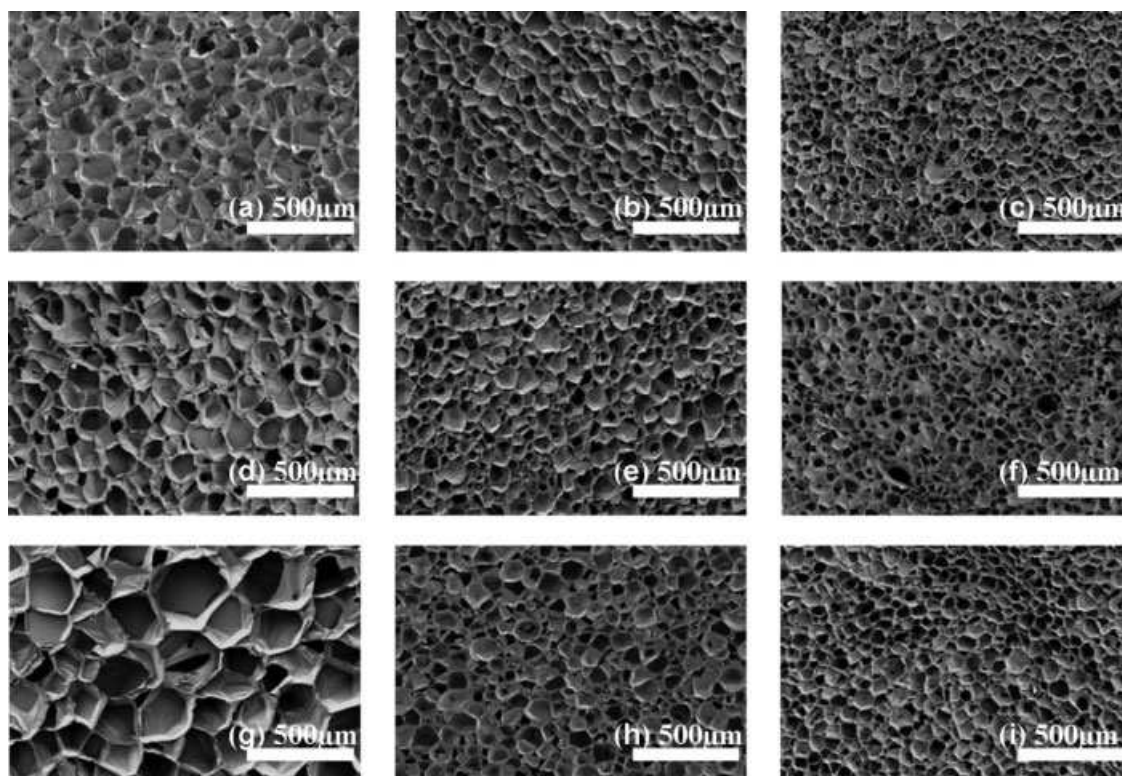


FIG. 8. SEM morphologies of semi-crystalline cPLA foams obtained with 5, 7, and 9% CO₂ (from left to right) and branched with 0, 1, and 2% CE (from top to bottom).

of achieved crystallinity during the foaming increased from 0 to 30%. For foams obtained from branched cPLA with 2% CE, the T_{ch} decreased with CO₂ concentration, from 112 down to 90°C. These values were slightly lower than in the case of the unbranched cPLA foams. The level of crystallinity in the branched foams also increased with CO₂ concentration but the level of crystallinity achieved for 9% CO₂, only 17%, was much lower than in the unbranched foams. The crystallinity levels were also measured for foamed samples branched with intermediate CE contents (results not shown here). For example, the crystallinity levels found in foams obtained from cPLA branched with 1.5% CE were 6, 20, and 22% respectively for 5, 7, and 9% CO₂. Therefore, the branched cPLA can also crystallize rapidly in the foaming process but the achieved crystallinity decreases with increasing CE content.

Typically, in the foaming process, a high extrusion temperature is used in the first step of the process to melt or soften the polymer. In our case, the barrel temperature was set to 190°C before the CO₂ injection point in all foaming-extrusion experiments. After the blowing agent injection point, the temperature was decreased with the purpose of increasing the melt strength of the polymer at die exit. The temperature must be decreased progressively with the increase in blowing agent concentration to take into account its plasticizing effect. In this study, an important finding was that the cPLA extrusion required a

higher mechanical energy input (i.e., higher screw torque) and, in consequence, the foaming temperature could not be lowered as much for cPLA than for aPLA. Figure 10 presents the minimum foaming temperature as a function of CO₂ concentration. The minimum achievable temperature was always limited by the extrusion screw torque limits. It was possible to decrease the aPLA foaming temperature from 190 down to 110°C at 9% CO₂. Similar foaming temperature was achieved at all CE contents. For cPLA, the minimum foaming temperature was much higher. The minimum foaming temperature of cPLA with 3 to 7% CO₂ was around 170°C. At 9% CO₂, the foaming temperature was between 130 and 160°C and, interestingly, it increased systematically with the CE content. It is assumed that the main difference in the minimum foaming temperature for amorphous and semi-crystalline PLA comes from crystallite formation before the die exit. Superimposed on this effect, the viscosity increase produced by the addition of the CE also increased the foam-

TABLE 2. Density of cPLA foams.

CE content	Density (kg/m ³)		
	5% CO ₂	7% CO ₂	9% CO ₂
0%	65	28	28
1%	43	37	30
2%	36	32	32

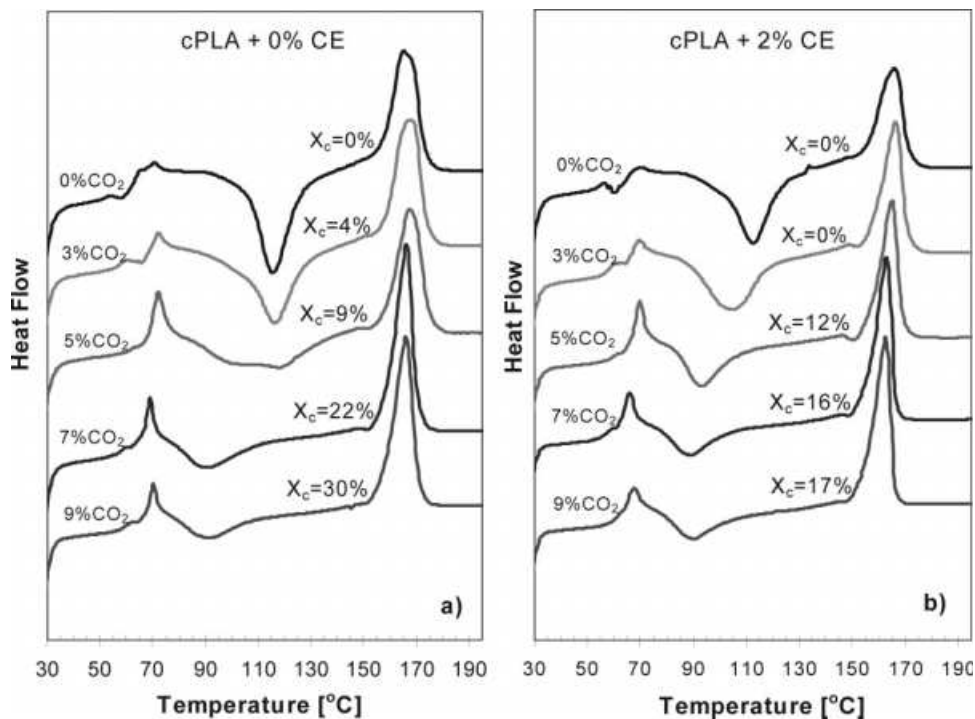


FIG. 9. DSC scans obtained upon the first heating of the pure (0% CE) and branched (2% CE) cPLA foamed with 3, 5, 7, and 9% CO₂.

ing temperature for the cPLA. It had no effect, however, on the foaming temperature of the amorphous aPLA. As we will see later, the low foaming temperatures achieved in the case of aPLA may have hindered the chain-branching reaction.

To confirm the presence of PLA crystallites prior to the die exit, the cell nucleation density was calculated based on the observed foam morphology. Figure 11 presents cell nucleation density as a function of CE content for foams with 5, 7, and 9% CO₂. For both PLA grades, the number of cells per unit volume increased greatly with CO₂ concentration but not with CE content. The most important feature is that the cPLA cell population density is always higher in comparison with aPLA at the same blowing agent concentration. By contrast to the cell nucleation in aPLA, the presence of crystalline nuclei formed before the die exit seemed to play a significant role in cPLA foam nucleation. The high screw torque and the higher cell nucleation density were indirect evidence of crystalline nuclei formation that occurred prior to the die exit. It was only with 9% CO₂ that the foam nucleation density of the amorphous material matched that of the semi-crystalline one.

PLA foams are characterized by a high number of open cells. Keeping in mind the possibility that crystallites were already present during the foam growth stage in cPLA cell walls, it is interesting to observe if the two PLA differ in terms of their rupture mechanism. Figure 12 presents high-magnification micrographs of one cell wall of aPLA (Fig. 12a and c) and of cPLA foams (Fig.

12b and d) obtained with 1% CE and 9% CO₂. For both PLA grades, cavitated structures were observed in cell walls that were ruptured as well as in unruptured ones (Fig. 12a and b). It discloses a network of very small cavities separated by fibrils. In some area, larger cavities with nonuniform dimensions have appeared due to the rupture

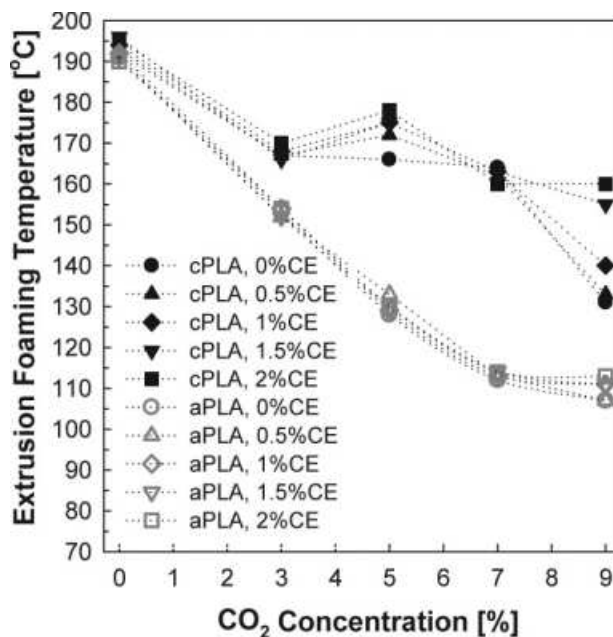


FIG. 10. Minimal extrusion temperature as a function of CO₂ concentration during the foaming of branched cPLA and aPLA.

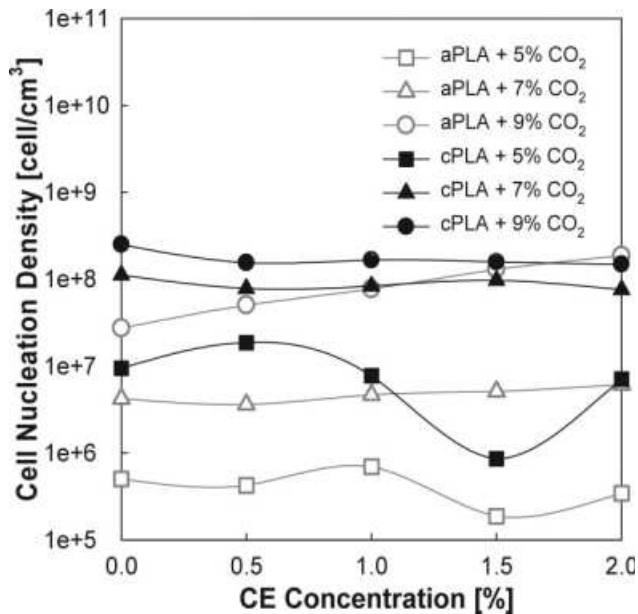


FIG. 11. Cell nucleation density as a function of chain extender concentration calculated for aPLA and cPLA foams obtained with 5, 7, and 9% CO₂.

of consecutive fibrils. Micrographs with higher magnifications are presented (Fig. 12c and d) to better describe the variety of cell wall textures and rupture types. The cavitated structures formed by aPLA and cPLA differed in the dimension of cavities, fibrils, and their orientation. Macrovoids of 0.5–1 μm in diameter were found in aPLA foam cell walls. These macrovoids were non-uniformly distrib-

uted, un-oriented and separated by fibrils with widths in 100–500 nm range. Much smaller cavities, 75–100 nm, were found in the case of cPLA. These cavities were separated by very short and thinner fibrils, around 10 nm, and very long ones that were thicker, in 50–100 nm range. It is around 10 times smaller than the cavities found for aPLA. The cavities were slightly elongated in the same direction as the thicker fibrils. It was postulated in our previous work that the cavitation took place in the amorphous zones between these crystallites [20, 21]. This supports the assumptions that the finer cavitated structure of cPLA is intimately related to the presence of crystalline domains in the cPLA cell walls. In aPLA, due to the lack of the crystallites, the cavitation phenomena took place arbitrarily, when the cell walls thickness was decreased down to a critical value during the cell growth. The weak points created in this way facilitated the rupture of the cell walls. Similar cell wall features were found for all chain-extender contents.

The unfoamed aPLA and cPLA presented a similar complex viscosity when the same CE content was added (see Fig. 3). It is interesting to examine how the viscosity of branched materials has evolved after the foaming process. Figure 13 presents complex viscosity at 180°C as a function of CE content for unfoamed aPLA, cPLA, and for foams obtained with 5% CO₂. The values chosen for complex viscosity correspond at a frequency of 1 rad/s. The samples obtained from aPLA foams showed a gradual increase in complex viscosity with CE content but this increase was lower than that for the unfoamed aPLA material. The foams obtained from cPLA with 5% CO₂, showed

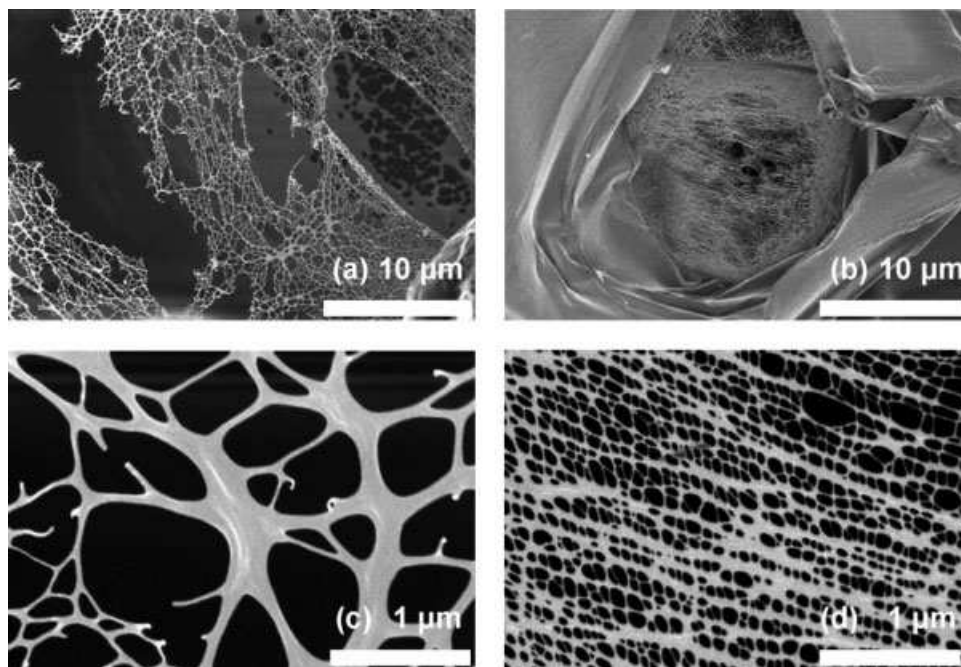


FIG. 12. Details of cell wall ruptures for (a) - aPLA foams obtained in the presence of 1% CE and 9% CO₂, (b) - cPLA in the presence of 1% CE and 9% CO₂. The micrographs (c) and (d) are higher magnifications of (a) and (b), respectively.

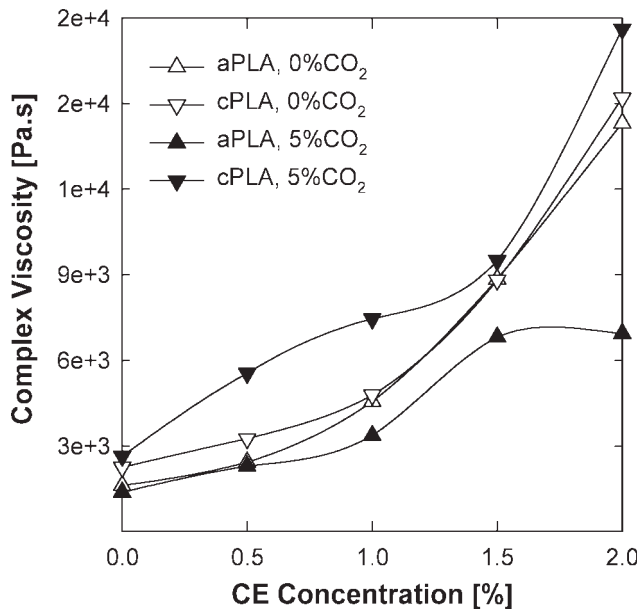


FIG. 13. Complex viscosity as a function of CE content for aPLA and cPLA unfoamed and foamed with 5% CO₂. The values correspond to a frequency of 1 rad/s for tests done at 180°C.

slightly higher complex viscosity values as for the unfoamed cPLA material. As showed by the continuous increase in complex viscosity, chain-branching was achieved during the extrusion foaming process for both PLA grades. Nevertheless, the level of branching was lower for aPLA foams than for cPLA foams. This can be explained by the lower foaming temperatures achieved during aPLA foaming. These lower temperatures limited the reactivity of the chain-extender. Therefore, it can be assumed that the chain-branching of aPLA was hindered by the lower temperature used after the CO₂ injection point. This assumption points to an interesting dilemma in the case of the amorphous foams. The lowering of foaming temperature is usually a way to improve the melt strength and improve the foam stability and overall quality. In the case of the reactive blend however, this improved stability comes at the expense of a decrease in branching reaction, also a rheological means to improve the foam stability. Further study would be required to identify the conditions for optimal foaming and branching.

Elongational viscosity measurements were also carried out on the samples prepared from PLA extruded foams. Figure 14 presents the elongational viscosity at 180°C of aPLA and cPLA foamed with 3, 5, and 9% CO₂. The CE content used in extrusion foaming was 2% in all the samples. The elongational viscosity of foams from unbranched PLA at a Hencky strain rate of 0.1 s⁻¹ are presented as reference in each graph. It showed a very low viscosity and no strain-hardening, similar to the reference materials presented in Fig. 5a–d. The chain-branched and foamed aPLA showed similar elongational viscosities and strain-hardening for all blowing agent concentrations

as can be observed in Fig. 14a, c, and e. The samples obtained from cPLA foams also showed strain-hardening but, the elongational viscosities presented some variations with CO₂ concentration (Fig. 14b, d, and f). These results show that the samples obtained from branched aPLA and cPLA foams presented, however, longer relaxation times due to the increased branching density and higher entanglement levels than for the unbranched foams. The aPLA and cPLA exhibited almost similar elongational viscosities in the melt state. This may be surprising considering the difference in foaming behavior for aPLA and cPLA. It must therefore be emphasized that the foaming conditions differ from the rheological measurement conditions. As we have shown, foaming provides conditions that are very favorable to crystallization. The crystallites can increase the viscosity of the cPLA material by acting as solid particles dispersed in the flowing amorphous matrix. This viscosity increase can add to the effect of chain-branching. Thus, a full description of the cPLA foaming process should take into account crystal growth as well as the purely rheological effects expressed by the transient elongational viscosity data.

CONCLUSIONS

Two different grades of PLA, an amorphous and a semi-crystalline one, were branched using an epoxy-styrene-acrylic copolymer as a reactive chain-extender. The mixing and reaction of the chain-extender with the PLA increased the shear viscosity, the melt elasticity and most importantly, caused strain-hardening upon uniaxial deformation in the molten state. Similar effects were observed when adding the chain-extender in foaming trials. In this case, the viscosity measurements carried out on the consolidated foamed sample showed that the chain-extension reaction was slightly hindered by the lower processing temperature used especially for foaming of the amorphous PLA. Nonetheless, the shear and elongational viscosity of samples obtained from the chain-extended foams were significantly higher than the non-modified controls. The increased melt elasticity and strength measured in controlled rheological experiments did not translate into a significant effect on the properties of CO₂-foamed PLA. For amorphous PLA, low-density foams were obtained only at 9% CO₂ content and similar foam morphologies were obtained regardless of the chain-extender content. By contrast, low-density foams could be produced with crystallizable PLA starting with only 5% CO₂. At this blowing agent concentration, the foam density was reduced from 65 to 30 kg/m³ by addition of the chain-extender showing in this case the benefit of the higher melt strength. At higher blowing agent concentration, however, low-density foams were obtained regardless of the chain-extender concentration. This showed that at these CO₂ levels, the rapid crystalline nucleation and growth than occur simultaneously with the foam cell growth played a role that essentially overwhelmed the effect of chain-

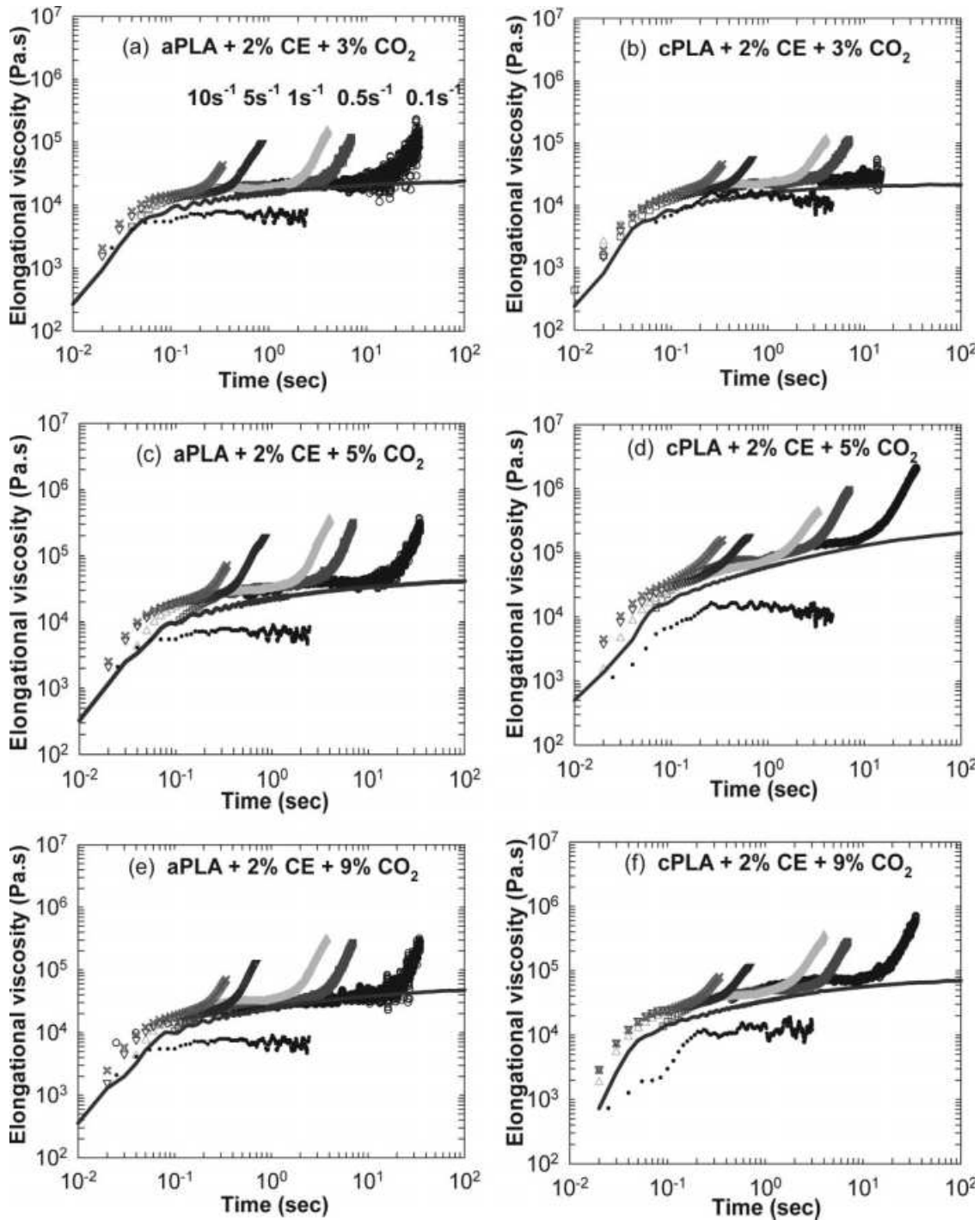


FIG. 14. Elongational viscosity as a function of time for foamed PLA branched with 2% chain extender. Strain rates were 0.1, 0.5, 1, 5, and 10 s^{-1} from right to the left. The continuous curves represent the stress growth functions ($3\eta^+$) obtained in shear.

extension. The crystalline PLA foams had higher foam nucleation density indirectly showing that PLA crystalline nuclei had contributed to the foam cell nucleation. It was also shown that in this CO_2 rich environment, PLA crystal nucleation may even start under pressure prior to die exit. This premature nucleation significantly increased the flow resistance and forced the use of much higher foam-

ing temperatures than for the amorphous material. It is noteworthy that in independent rheological tests, the amorphous and crystalline PLA exhibited relatively similar viscosity levels. Therefore, it was clearly the different thermal behaviors that caused the differences in processability. A second indirect evidence of simultaneous crystallization and foam cell growth came from the close ex-

amination of ruptured foam cell walls which showed very finely cavitated structures in the crystalline foams typical of a crystalline/amorphous heterogeneity scale.

ACKNOWLEDGMENTS

The authors would like to acknowledge the financial contribution of the Natural Science and Engineering Council of Canada and the technical support provided by Pierre Sammut, Chantal Coulombe, Yves Simard, and Michel Carmel from the Industrial Materials Institute, National Research Council of Canada.

REFERENCES

1. R. Auras, B. Harte, and S. Selke, *Macromol. Biosci.*, **4**, 835 (2004).
2. R. Auras, S.P. Singh, and J. Singh, *J. Test. Eval.*, **34**, 1 (2006).
3. L.T. Lim, R. Auras, and M. Rubino, *Prog. Polym. Sci.*, **33**, 820 (2008).
4. D. Garlotta, *J. Polym. Environ.*, **9**, 63 (2001).
5. Michel F. Champagne and R. Gendron, "Rheological Behavior Relevant to Extrusion Roaming," in *Thermoplastic Foam Processing: Principles and Development*, S.T. Lee, Ed., CNRC Press, Boca Raton, FL, 43 (2005).
6. C.F.J. Den Doelder, R.L. Sammler, R.J. Koopmans, and A.N. Paquet, *Cell Polym.*, **21**, 99 (2002).
7. I. Pesneau, M. Champagne, R. Gendron, and M.A. Huneault, *J. Cell Plast.*, **38**, 421 (2002).
8. R. Gendron and C. Vachon, *J. Cell Plast.*, **39**, 71 (2003).
9. J. Stange and H. Münstedt, *J. Rheol.*, **50**, 907 (2006).
10. H. Munstedt, S. Kurzbeck, and J. Stange, *Macromol. Symp.*, **245**, 181 (2006).
11. P. Potschke, B. Krause, J. Stange, and H. Munstedt, *Macromol. Symp.*, **254**, 400 (2007).
12. A. Sodergard and J.H. Nasman, *Ind. Eng. Chem. Res.*, **35**, 732 (1996).
13. D.H.S. Rankumar and M. Bhattacharya, *Polym. Eng. Sci.*, **38**, 1426 (1998).
14. J.J. Cooper-White and M.E. Mackay, *J. Polym. Sci. Part B: Polym. Phys.*, **37**, 1803 (1999).
15. J.R. Dorgan and J.S. Williams, *J. Rheol.*, **43**, 1141 (1999).
16. J.R. Dorgan, H. Lehermeier, and M. Mang, *J. Polym. Environ.*, **8**, 1 (2000).
17. H. Lehermeier and J.R. Dorgan, *Polym. Eng. Sci.*, **41**, 2172 (2001).
18. E.-S. Kim, B.C. Kim, and S.H. Kim, *J. Polym. Sci. Part B: Polym. Phys.*, **42**, 939 (2004).
19. J. Reignier, R. Gendron, and M.F. Champagne, *Cell Polym.*, **26**, 83 (2007).
20. M. Mihai, M.A. Huneault, B.D. Favis, and H. Li, *Macromol. Biosci.*, **7**, 907 (2007).
21. M. Mihai, M.A. Huneault, and B.D. Favis, *J. Appl. Polym. Sci.*, **113**, 2920 (2009).
22. L.-I. Palade, H. Lehermeier, and J.R. Dorgan, *Macromolecules*, **34**, 1384 (2001).
23. H. Yamane, K. Sasai, M. Takano, and M. Takahashi, *J. Rheol.*, **48**, 599 (2004).
24. L. Incarnato, P. Scarfato, L. Di Maio, and D. Acierno, *Polymer*, **41**, 6825 (2000).
25. F. Awaja, F. Daver, and E. Kosior, *Polym. Eng. Sci.*, **44**, 1579 (2004).
26. J.S. Forsythe, K. Cheah, D.R. Nisbet, R.K. Gupta, A. Lau, A.R. Donovan, M.S. O'shea, and G. Moad, *J. Appl. Polym. Sci.*, **100**, 3646 (2006).
27. S. Japon, A. Luciani, Q.T. Nguyen, Y. Leterrier, and J.A.E. Manson, *Polym. Eng. Sci.*, **41**, 1299 (2001).
28. M. Xanthos, C. Wan, R. Dhavalikar, G.P. Karayannidis, and D.N. Bikiaris, *Polym. Int.*, **53**, 1161 (2004).
29. R. Dhavalikar and M. Xanthos, *J. Appl. Polym. Sci.*, **87**, 643 (2002).
30. R. Dhavalikar and M. Xanthos, *Polym. Eng. Sci.*, **44**, 474 (2004).
31. M. Xanthos and M.-W. Young, *Polym. Eng. Sci.*, **41**, 643 (2001).
32. W. Zhong, J. Ge, Z. Gu, W. Li, X. Chen, Y. Zang, and Y. Yang, *J. Appl. Polym. Sci.*, **74**, 2546 (1999).
33. B.-H. Li and M.-C. Yang, *Polym. Adv. Technol.*, **17**, 439, (2006).
34. J. Ren, Q.-F. Wang, S.-Y. Gu, N.-W. Zhang, and T.-B. Ren, *J. Appl. Polym. Sci.*, **99**, 1045 (2006).
35. J. Borda, I. Bodnar, S. Keki, L. Sipos, and M. Zsuga, *J. Polym. Sci. Part A: Polym. Chem.*, **38**, 2925 (2000).
36. J. Kylma, J. Tuominen, A. Helminen, and J. Seppala, *Polymer*, **42**, 3333 (2001).
37. J. Tuominen, J. Kylma, and J. Seppala, *Polymer*, **43**, 3 (2002).
38. S.Y. Gu, M. Yang, T. Yu, T.B. Ren, and J. Ren, *Polym. Int.*, **57**, 982 (2008).
39. K. Hiltunen, J.V. Seppala, and M. Harkonen, *J. Appl. Polym. Sci.*, **64**, 865 (1997).
40. M. Champagne, R. Gendron, and M.A. Huneault, *Proc. SPE ANTEC*, Nashville, TN, 1870 (2003).
41. M. Villalobos, A. Awojulu, T. Greeley, G. Turco, and G. Deeter, *Energy*, **31**, 3227 (2006).
42. V. Karayan and M. Villalobos, *Proc. Global Plast. Env. Conf.*, **52** (2004).
43. M.L. Sentmanat, *Rheol. Acta*, **43**, 657 (2004).
44. M.L. Sentmanat, B.N. Wang, and G.H. McKinley, *J. Rheol.*, **49**, 585 (2005).
45. Y. Sato, K. Inohara, S. Takishima, H. Masuoka, M. Imaizumi, H. Yamamoto, and M. Takasugi, *Polym. Eng. Sci.*, **40**, 2602 (2000).
46. E.W. Fischer, H.J. Sterzel, and G. Wegner, *Kolloid-Z. u. Z. Polym.*, **251**, 980 (1973).